ACSNANO

www.acsnano.org

ARTICLE

Steering Micromotors via Reprogrammable Optoelectronic Paths

Xi Chen, Xiaowen Chen, Mohamed Elsayed, Harrison Edwards, Jiayu Liu, Yixin Peng, H. P. Zhang,* Shuailong Zhang,* Wei Wang,* and Aaron R. Wheeler*

Cite This: https://doi.org/10.1021/acsnano.2c12811

Read Online

ACCESS | Metrics & More | Article Recommendations | Supporting Information

ABSTRACT: **Steering micromotors is important for using them in practical applications and as model systems for active matter. This functionality often requires magnetic materials in the micromotor, taxis behavior of the micromotor, or the use of specifically designed physical boundaries. Here, we develop an optoelectronic strategy that steers micromotors with programmable light patterns. In this strategy, light illumination turns hydrogenated amorphous silicon conductive, generating local electric field maxima at the edge of the light pattern that attracts micromotors via positive dielectrophoresis. As an example, metallo-dielectric Janus microspheres that self-propelled under alternating current electric fields were steered by static light patterns along customized paths and through complex microstructures. Their long-term directionality was also rectified by ratchet-shaped light patterns. Furthermore, dynamic light patterns that varied in space and time enabled more advanced motion controls such as multiple motion modes, parallel control of multiple micromotors, and the collection and transport of motor swarms. This optoelectronic steering strategy is highly versatile and compatible with a variety of micromotors, and thus it possesses the potential for their programmable control in complex environments.**

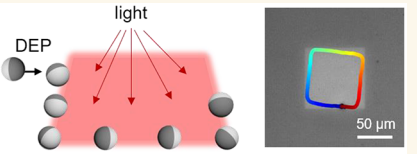

KEYWORDS: *micromotor, optoelectronic tweezers, dielectrophoresis, confinement, direction control*

INTRODUCTION

Micromotors that convert local or external energy into autonomous motion have drawn much attention over the past two decades.[1−5] From a fundamental perspective, micromotors are useful for the study of the nonequilibrium thermodynamics and active matter because of their similarity with biological microswimmers.[6−8] From an applied perspective, micromotors are prototypical miniaturized machines capable of performing tasks such as drug delivery,[9,10] cargo transportation,[11,12] environmental remediation,[13] and microfabrication.[14] However, micromotors typically move in random trajectories because of thermal fluctuations, while applications in complex environments require them to move along predefined and precise paths. The development of steering strategies is thus a key element in micromotor research.[15−20]

Several strategies are available to steer micromotors. The most common one uses an external magnetic field to steer micromotors that are made of magnetically responsive materials (see refs 21−25 for examples). However, precise and sophisticated magnetic steering often requires complicated magnetic setups (such as a Helmholtz coil). More importantly, due to the limitation of magnetic field, all motors are steered simultaneously and in the same way, making it difficult to control multiple motors independently. Alternatively, micromotors can respond to chemical gradients[26] or light gradients[27]/direction[28] and migrate accordingly,[29,30] i.e., chemotaxis and phototaxis. Unfortunately, only specialized micromotors that are sensitive to chemical gradients or light gradients/direction can taxis efficiently. More recently, boundaries have proved to be yet another effective way to steer micromotors, which either move closely to and along physical walls[31−40] or become confined by tweezing flows near flat interfaces that serve as virtual walls.[41] Constructing microstructures of specific shapes can therefore guide a micromotor to move in a specific trajectory, without the need for an external magnetic field or gradient. However, steering micromotors with physical boundaries also has some limitations. First, building a microstructure requires complex and costly microfabrication processes such as photolithography[39,40] or two photon nanolithography.[31] Second, once fabricated, the boundary is fixed and cannot dynamically turn the trajectories of micromotors. Given the above limitations of each steering strategy, there is continued need for alternative strategies that can be generically applied to all kinds of micromotors, are highly precise, versatile and programmable, and can change in space and time.

Received: December 28, 2022
Accepted: March 6, 2023

Toward this goal, we here report an optoelectronic steering strategy that guides the movement of micromotors along programmable paths with dynamic light patterns. The optoelectronic effect has been exploited extensively in optoelectronic tweezers (OET) to manipulate microparticles and cells.[42] The key device of this technology is a photoconductive substrate that switches from being an insulator to a conductor upon irradiation of light of proper wavelengths. When an electric field is applied vertical to the photoconductive substrate, the electric field's strength reaches its maximum at the edges of the light pattern. Micromotors are thus confined by dielectrophoresis to the pattern edge while self-propelling, allowing for their precise steering. We describe below in detail how static light patterns control the trajectory and directionality of a micromotor and how dynamic light patterns cause micromotors to move in multiple motion modes as well as their ensemble transport. These examples portray metallo-dielectric micromotors that self-propel via induced charge electrophoresis (ICEP) under an alternating current (AC) electric field, which serve as the source both for the power and for dielectrophoresis. However, catalytic micromotors that move by chemical reactions were also steered by this strategy, proving its generalizability. Compared with conventional steering strategies that use magnetic fields, taxis, or physical boundaries, the optoelectronic steering strategy has the advantages of being flexible and reconfigurable, and thus it is particularly well-suited to precisely manipulate one or many micromotors in a complex and changing environment.

RESULTS/DISCUSSION

Micromotors and Light Patterns on a Photoconductive Substrate: Basic Properties. We begin by describing the basic features of our optoelectronic setup and the micromotors used. Figure 1a shows the schematic of the experimental setup of an optoelectronic system. Red light of 625 nm of power density up to 2960 mW/cm^2 was passed through a digital micromirror device (DMD), which generated structured light patterns that were focused on a photoconductive substrate via an upright optical microscope. This substrate is a key component of the experiment and contains a 1 μm layer of hydrogenated amorphous silicon (a-Si:H) on top of an indium tin oxide (ITO) glass slide. a-Si:H is a photoconductive material that becomes conductive upon irradiation of red light but otherwise remains insulating.[43] A sealed experimental chamber of 200 μm height was placed above the substrate and held a suspension of metallo-dielectric microspheres suspended in 0.1 mM NaCl liquid medium. These particles were prepared by sputtering 10 nm of Pt on SiO_2 microspheres of 5 μm in diameter (referred to as SiO_2-Pt micromotors, see Figure S1 for a scanning electron microscope image). They move in an AC electric field toward the SiO_2 hemisphere via induced charge electrophoresis (ICEP)[44−48] (Figure 1b), which originates from the asymmetric electroosmotic flow on the Pt and the SiO_2 hemisphere that polarize differently in the same electric field. A detailed propulsion mechanism can be found in refs 48 and 49 but is beyond the scope of this study.

These SiO_2-Pt micromotors then moved upon applying AC electric fields between two ITO slides typically oscillating at 100 kHz. Notably, because illuminated a-Si:H patches become electrically conductive, a SiO_2-Pt micromotor, which moves faster in stronger electric fields (Figure S3), moved significantly faster in a light pattern than regions that were not illuminated ("dark"). This is qualitatively compared in Figure 1c, d and Video S1. Therefore, we consider them "immotile" when outside of a light pattern for the remainder of this article. Although not important for steering discussed below, the speeds of SiO_2-Pt micromotors can be readily tuned by adjusting the applied voltage and/or light intensity (Figure S4), which ultimately affects the electric field strength a motor experiences and thus the magnitude of ICEP and the associated propelling force. Note that a high oscillating frequency of 100 kHz (or less commonly 75 kHz) was used throughout this article to reduce the effects caused by ions, such as electrode polarization that screens applied potentials,[50] electrochemical reactions on the electrode surfaces,[51] or electroosmosis,[52] that could become significant at lower frequencies.

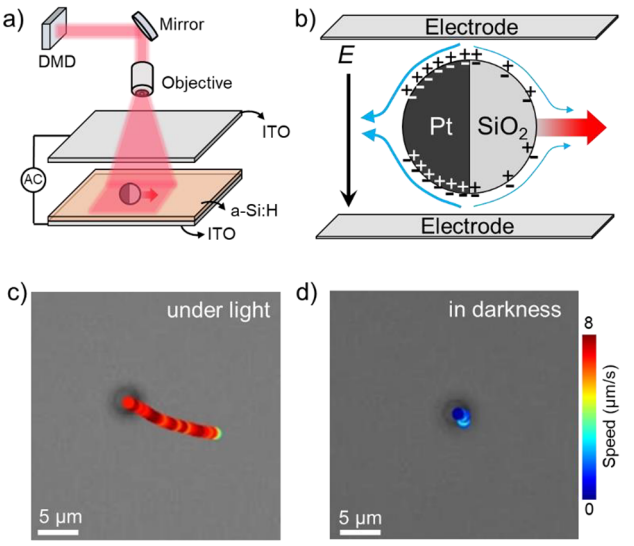

Figure 1. SiO_2-Pt Janus micromotors in an optoelectronic tweezer setup. (a) Schematic of the optoelectronic device. Structured light generated by a digital micromirror device (DMD) is projected on a photoconductive substrate composed of a layer of hydrogenated amorphous silicon (a-Si:H) on a glass slide coated with indium tin oxide (ITO). An alternating current (AC) electric field is applied between two ITO slides. (b) Proposed propulsion mechanism of a SiO_2-Pt micromotor. The Pt and SiO_2 hemispheres polarize differently under an electric field (black arrow), generating induced-charge electroosmotic flows (blue arrows) of different magnitudes. The motor thus moves in the direction of its SiO_2 hemisphere. Only one half cycle is shown for AC electric fields; the motor moves in the same direction in both cycles. (c and d) Time-lapsed optical micrographs illustrating representative trajectories over 2.8 s for SiO_2-Pt motors inside (c) and outside (d) light patterns, taken from Video S1. Tracked velocities (red, high; blue, low) are superimposed on the images. Experimental conditions: AC electric fields at 100 kHz and 5 V_{p-p} were used, and light intensity was 2690 mW/cm^2.

Dielectrophoresis Confines Micromotors to the Interface between the Illuminated and Dark Areas. A key observation is the preferred confinement of SiO_2-Pt micromotors at the edge of a light pattern (i.e., the interface between the illuminated and dark areas). As an example, Figure 2 and Video S2 show that a SiO_2-Pt micromotor, placed either outside or inside a light pattern to begin with, was attracted toward the pattern's edge upon turning on the light. Once close to the interface, the SiO_2-Pt motor self-propelled along the edge by reorienting its Janus interface perpendicular to the

https://doi.org/10.1021/acsnano.2c12811
ACS Nano XXXX, XXX, XXX−XXX

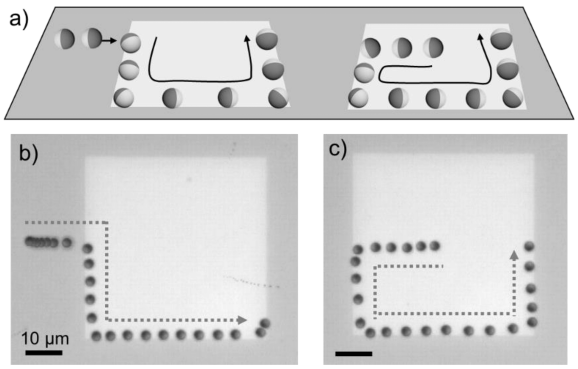

Figure 2. SiO_2-Pt micromotors confined to and moving along an OET light pattern. (a) Schematic illustrating the movement of a micromotor (Pt, dark gray; SiO_2, light gray) toward and along the edge of a square light pattern approaching the edge from the outside (left) and the inside (right). (b and c) Time-lapsed optical micrographs corresponding to (a), taken from Video S2. Experimental conditions: AC electric fields of 100 kHz and 10 V_{p-p}, and a light pattern of 100 μm × 100 μm at 2960 mW/cm^2.

patten's edge. It then continuously traced the entire pattern contour. Notably, the speed of a micromotor that started from within the light pattern increased from ~20 to ~32 μm/s upon moving close to the pattern's edge. As we show below in Figure 3e and 3f, this acceleration is consistent with the higher electric field strength at the pattern's edge than its center.

The preferred confinement of a micromotor to a light pattern's edge, the cornerstone that we build our steering strategy around, can be explained by positive dielectrophoresis (DEP). DEP is the directed transport of an electrically polarizable particle in a gradient of electric field,[53−55] and positive DEP refers migration up the gradient. The magnitude of the DEP force F_{DEP}, whether positive or negative, of a sphere is given (to the leading order) by[55]

$$F_{DEP} = 4\pi\varepsilon_m R^3 \mathrm{Re}(K)\nabla E^2 \quad (1)$$

where R is the microsphere radius, ε_m is the permittivity of the medium, Re(K) is the real component of the Clausius−Mossotti factor K (related to the electrical polarizability of the particle), and E is the electric field strength. Note that eq 1 uses a point-dipole approximation, which assumes that the particle is small compared with the spatial inhomogeneities of the electric field.

Specific to our experiments, we propose that a metallo-dielectric micromotor (such as SiO_2-Pt used here) undergoes positive dielectrophoresis to the pattern's edge where the electric field strength is the highest. A schematic is shown in Figure 3a and b. This proposed DEP trapping mechanism is supported by the following evidence. First, we confirm in Figure 3c that a 5 μm SiO_2-Pt microsphere undergoes positive DEP, manifested by its positive electrical polarizability (i.e., positive Re(K)) across a wide range of driving frequencies, including 100 kHz used here. The detailed calculation is given in the Supporting Information. Similarly, pure SiO_2 or metal microspheres of positive Re(K) both accumulate at the light pattern's edge in the same way as a SiO_2-Pt micromotor (Figure S6). Second, a simulation model was built to study the distribution of electric field in the OET system, and Figure 3d shows the model configuration. The simulation results in Figure 3e and f show that the electric field norm reaches its maximum at the edge of the light pattern, with an electric field strength roughly twice as high as that at the light pattern's center (Figure 3g). Therefore, a SiO_2-Pt micromotor is attracted to the edge of a light patten by positive dielectrophoresis.

Dielectrophoresis alone, however, predicts that a SiO_2-Pt micromotor would stall at the light pattern's edge, because it prefers to align its Janus interface flush with the light pattern's edge so that its metal hemisphere, which polarizes more strongly than the dielectric hemisphere, points toward the electric field maximum. This is inconsistent with the observation in Figure 3b that a SiO_2-Pt micromotor self-propelled along the light pattern's edge. The phenomenon of guided motion of Janus particles can be explained by the rotation of Janus particles in an electric field. The electric field induces two effects that result in the rotation of Janus particles. First, the electric field polarizes Janus particles and induces a dipole moment that is parallel to the boundary separating the two hemispheres. This dipole moment prefers to align with the direction of the electric field as it maximizes the polarization and minimizes the electrical energy (See Figure 3b for a schematic and Figure S5 for an example of such an alignment of a Janus particle in an external electric field).[56,57] Second, hydrodynamic torque resulting from the electroosmotic flow also contributes to the alignment of the Janus micromotor, thereby maintaining its orientation.[58] As a result, the vertical component of the electric field (E_z) in the OET system can cause out-of-plane rotation of a SiO_2-Pt micromotor in the horizontal plane so that the Janus structure of the micromotor aligns parallel to the E_z line and stably swims. We also note the presence of a strong, horizontal component of the electric field (E_x in Figure 3g) across the light−darkness interface. Its magnitude quickly rises from 0 at the pattern's center to 9 × 10^4 V/m (Figure 3g) at its edge. The E_x can predominantly influence the in-plane rotation and control the self-propelled direction of the micromotor in the horizontal plane, making it swim along the edge of the light pattern as observed in the experiment.

Controlling Micromotor Trajectories with Static Light Patterns. The discovery that micromotors are dielectrophoretically confined to the edges of a light pattern enables the control over the trajectory and moving directions of one or more micromotors. Figure 4 shows a few basic controls achieved with static light patterns, i.e., those that do not change in space or time. Examples of controlled trajectories include a straight line (vs diffusive trajectories typical for micromotors) in a narrow light pattern (Figure 4a, b), and trajectories following the contours of light patterns of various simple shapes (Figure 4c), letters (Figure 4d), or even complex shapes such as a crossed serpentine (Figure 4e). Moreover, Figure 4f shows that multiple micromotors can be controlled in parallel to move in completely different trajectories, a challenging task for motors steered by magnets or taxis. Furthermore, Figure 4g shows that a micromotor can be optoelectronically guided through complex physical landscape/maze/barriers, such as a photolithographically fabricated microstructure. Finally, Figure 4h and i show that ratchet-shaped light patterns can rectify an otherwise Brownian micromotor to move in clockwise or counterclockwise circles. The rectification of the direction of a micromotor is related to the heart-shaped element of the light pattern. For instance, in the light pattern shown in Figure 4h, when the OET system is activated, the micromotor is attracted to the edge of the light pattern. At this point, the micromotor's clockwise or

https://doi.org/10.1021/acsnano.2c12811
ACS Nano XXXX, XXX, XXX−XXX

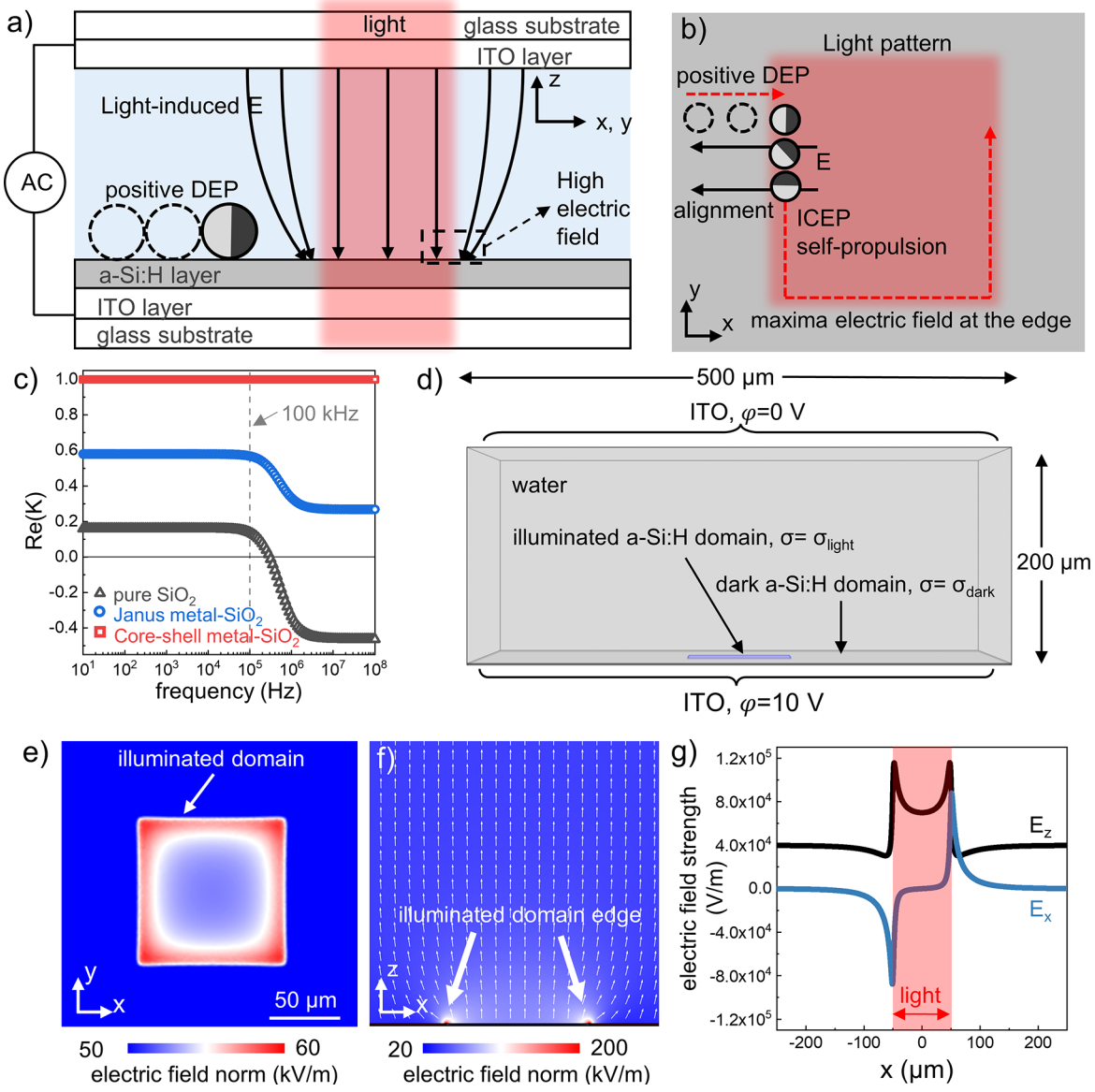

Figure 3. Dielectrophoretic confinement of a Janus SiO_2-Pt micromotor at the edge of light pattern. (a) Schematic of the operating principle of positive dielectrophoresis (DEP) in an OET device. Light (pink) irradiated on a photoconductive a-Si:H substrate greatly increases its electrical conductivity, generating electric field strength maxima at the edge of the light pattern. A colloidal particle more polarizable than its surrounding medium, such as a SiO_2-Pt Janus microsphere (Pt, dark gray; SiO_2, light gray), migrates toward the electric field maxima by positive DEP. (b) x–y plane of the OET device: once close to the edge of the light pattern, the Janus micromotor aligns itself and moves along the edge due to ICEP. One half a cycle of an AC electric field is shown in (a) and (b) for illustrative purpose. (c) Plots of the real component of the Clausius–Mossotti factor (Re(K)) as a function of frequency for three types of 5 μm diameter microspheres: SiO_2 (gray triangles), SiO_2 coated with a metal shell (red squares), and a SiO_2-Pt Janus microsphere (blue circles). See Supporting Information for calculations. (d) COMSOL Model configuration to simulate the electric field for a 100 μm × 100 μm light pattern projected into an OET device. (e) Top-view plots of the simulated electric field norm (blue, low; red, high) for a 100 μm × 100 μm light pattern projected into an OET device. (f) Side-view plot of the simulated electric field norm of the same light pattern (arrows represent normalized electric fields in the x and z dimensions, not to scale). See Figure S2 for more results. (g) Plots of the x and z components of the simulated electric field strength (E_x, blue; E_z, black) plotted along a line cross-sectioning the light pattern in the x dimension in (d), located 2.5 μm above the substrate in the z dimension. Positive values in E_x and E_z are along the positive axes.

counterclockwise movement is random. However, if the micromotor moves counterclockwise, it changes direction from counterclockwise to clockwise upon encountering the heart-shaped area. This specific pattern shape can turn the micromotor around by aligning the Janus micromotor with the light pattern's edge as mentioned before. Once the micromotor begins moving clockwise, it will continue to do so throughout the light pattern. In contrast, if the light pattern is a simple circle, the micromotor's clockwise or counterclockwise movement is random (Figure S7).

These results demonstrate the simplicity, flexibility, and versatility of using light patterns and associated light-induced dielectrophoresis to steer micromotors and control their motions.

Trajectory Control and Swarm Transport of Micromotors by Dynamic Light Patterns. A distinct advantage of

https://doi.org/10.1021/acsnano.2c12811
ACS Nano XXXX, XXX, XXX–XXX

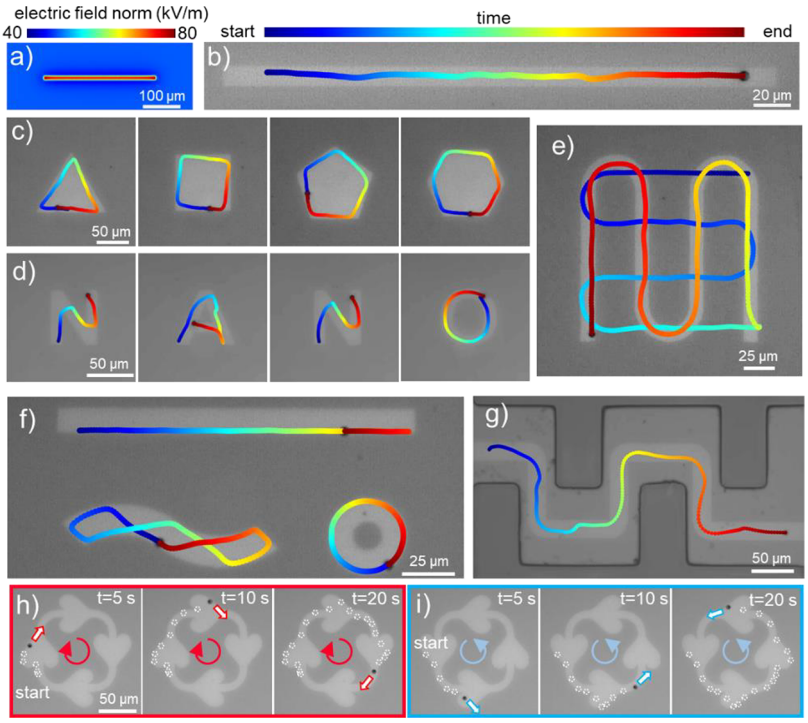

Figure 4. SiO_2-Pt micromotors steered by static light patterns (Video S3). (a) Optical micrograph of linear pattern projected into an OET device with superimposed electric field (high, red; low, blue). (b–g) Time-lapsed optical micrographs of light patterns (b: line; c: sequential triangle, square, pentagon, hexagon; d: sequential letters spelling "NANO"; e: sequential horizontal then vertical serpentine patterns; f: parallel line, squiggle, doughnut; g: corrugated pattern in a physical microchannel) in an OET device with superimposed particle trajectories (start, blue; end, red). (h and i) Time-lapsed optical micrographs of a micromotor rectified to move in clockwise (h, red arrowhead) and counterclockwise (i, blue arrowhead) circles by rachet-shaped light patterns. Past locations are indicated by white circles. Experimental conditions: AC electric fields of 100 kHz (75 kHz for (d)) and 10 $V_{p\text{-}p}$; light intensity of 2960 mW/cm^2.

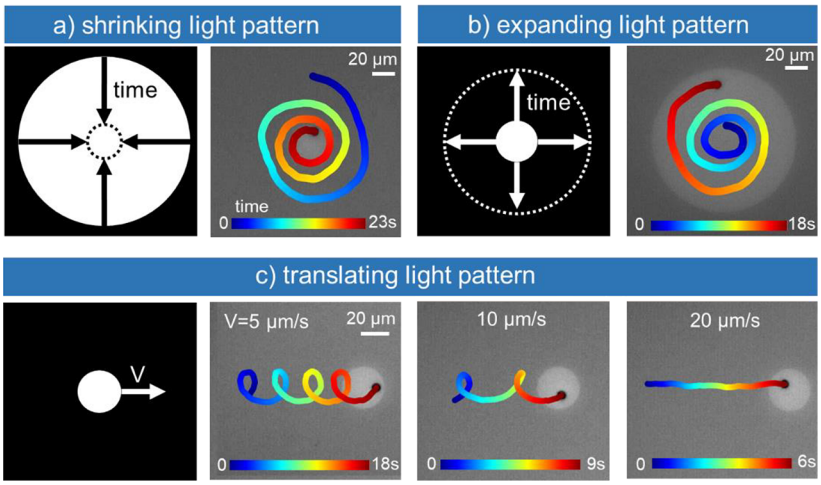

Figure 5. Spiral, helical, and linear motion of a micromotor in dynamic light patterns (Video S4). (a and b) Schematics (left) and time-lapsed optical micrographs with superimposed trajectories (start, blue; end, red) (right) of spiraling motion of a micromotor in a circular light pattern that shrinks (a) or expands (b) at 4 μm/s. (c) Schematic (left) and time-lapsed optical micrographs with superimposed trajectories (start, blue; end, red) (right) of micromotors in a circular light pattern that translates to the right at velocity v = 5, 10, or 20 μm/s. Experimental conditions: AC electric fields of 75 kHz and 10 $V_{p\text{-}p}$; light intensity of 2960 mW/cm^2.

structured light generated by a DMD is its capability to change in space and time. Below we take advantage of this feature to generate dynamic light patterns that not only confine a micromotor but also modulate its modes of motion and transport them in space, which could prove useful in complex and changing environments.

First, Figure 5a and b show that a micromotor confined by a circular light pattern can be made to move inward or outward along a spiraling trajectory when the light pattern shrinks or expands, respectively. This is a result of a micromotor always moving at the edge of the light pattern, so that its tangential velocity remains constant but the radius of its circular trajectory decreases over time. The angular velocity and the pitch length of this spiraling motion can be precisely controlled by the speed of the motor and that of the increase/decrease of the light pattern's radius (results not shown). Second, a

https://doi.org/10.1021/acsnano.2c12811
ACS Nano XXXX, XXX, XXX–XXX

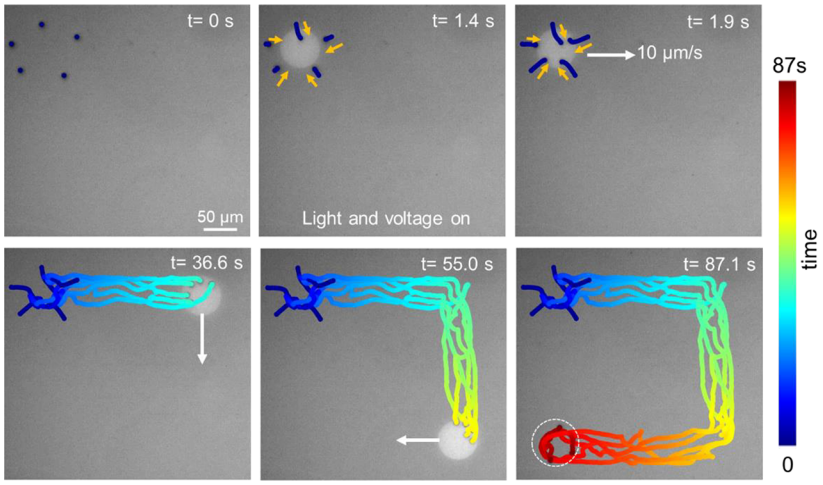

Figure 6. Collection and transport of five SiO_2-Pt micromotors by a dynamic light pattern (Video S5). Optical micrographs collected at different times *t* (top right corner) of a circular light pattern moving along three edges of a square (white arrowheads) at a constant velocity of 10 μm/s. Trajectories of each micromotor are color-coded in elapsed time (start, blue; end, red). The rough location of the light spot at *t* = 87.1 s (just before the light was turned off) is marked by a dashed circle. Experimental conditions: AC electric fields of 75 kHz and 10 V_{p-p}; light intensity of 2960 mW/cm^2.

circular light pattern that moves linearly causes trapped micromotors to move in helically shaped trajectories (Figure 5c), with a pitch length increasing with the speed of the light pattern. Interestingly, the motor no longer moves in helices but instead in straight lines when the light pattern moves beyond a critical speed. At this point the motor is essentially dragged forward by the back edge of the light pattern so that both move at the same speed.

Finally, the optoelectronic effect can also collect and transport multiple micromotors to a predefined location, building upon the knowledge we discussed above: micromotors are attracted to the edge of a light pattern and move along when the light pattern moves. This is demonstrated in Figure 6, where five individual micromotors were first collected by a circular light pattern. The light pattern then moved for hundreds of micrometers in arbitrary trajectories, transporting the trapped motors with it. More advanced operations can be envisioned (but not attempted), such as individual trapping and transport of any number of micromotors along complex yet independent trajectories. Once reaching their destinations, these micromotors can then move in different directions and at different speeds, enabled again by light patterns of different shapes, speeds, and light intensities.

DISCUSSION

In this section, we discuss the relevance of our work to optoelectronic tweezers, and we compare the optoelectronic steering reported here with steering by physical boundaries. We then show that optoelectronic steering can be applied to other kinds of micromotors, and we comment on its usefulness in the study of micromotors in confined environments.

First, there is a large body of research that uses optoelectronic tweezers (OET) for manipulating micro-objects such as micro-/nanoparticles, microrobots, and cells.[42] Both our work and other OET works rely on the same light-induced nonuniform electric fields and achieved seemingly similar trapping and controlled transport of micro-objects along predefined trajectories.[59−61] However, one of the main distinctions of the current work from other OET works is the target being manipulated. A typical OET work handles passive (immotile) micro-objects such as tracer microspheres,[62−64] microfabricated structures,[65−67] or even cells.[68−71] Although the DEP force in the OET system provides high motility of microparticles for various applications, their transport often requires the use of moving light patterns or substrates that exert pushing or dragging forces. Moreover, if multiple micro-objects need to move in a to-and-fro manner to perform a task, using OET force alone to achieve this goal requires feedback control to identify and regulate these micro-objects' movement. On the other hand, the micromotors used in our work *self-propel*, so that static light patterns alone are enough to *guide*, rather than to *force*, them to move toward a destination, making them more facile and flexible. Perhaps the optimal approach to control the micromotor is to combine the advantages of both the OET force and the self-propulsion force of the micromotor. For example, the OET force could be utilized to drag the micromotor to a target area at a long distance and high speed. Then, a light pattern could be introduced to precisely guide the micromotor to swim and self-propel within this target area.

Optoelectronic steering and a typical OET operation also differ in the nature of the trapping forces. For typical OET, microparticles are trapped by a combination of dielectrophoresis and AC electroosmotic flows (ACEOs).[72−74] In particular, ACEO arises from the coupling between a horizontal electric field and a charged substrate, and it converges inward so that a microparticle is hydrodynamically trapped to the center of a light pattern. We have however neglected the contribution of ACEO in steering micromotors in our experiments for two reasons. First, ACEO reaches its maximum at a critical charging frequency f_c, above which ions cannot follow the change in the electric field directions and cannot generate strong electroosmotic flows. f_c is given by[42]

$$f_c = \frac{\sigma_m \lambda_D}{2\pi\varepsilon L} \tag{2}$$

where σ_m and ε are the conductivity and permittivity of the medium, λ_D is the thickness of the electrical double layer (i.e., the Debye length), and L is the chamber height. In our

https://doi.org/10.1021/acsnano.2c12811
ACS Nano XXXX, XXX, XXX−XXX

experiment in 0.1 mM NaCl solution (see explanation of choosing this medium liquid in the SI file), f_c = 280 Hz, orders of magnitude smaller than the typical driving frequency of 100 kHz. We thus suspect ACEO to be exceedingly weak. In addition, ACEOs that converge from all sides typically confine particles at the center of a light pattern, inconsistent with our observation that particles are confined at the edges. It is then reasonable to assume that the contribution of ACEO in our experiments was small. We note, however, that micromotors deviated from the light pattern's edge (results not shown) at low driving frequencies of 50 kHz or lower, revealing the possible contributions of ACEO. Such deviation complicates precise steering and, therefore, is not discussed in this article.

Phenomenologically, the confinements shown in Figure 5 are similar to earlier reports of micromotors moving near physical boundaries.[32,33,39,40] In both cases, a micromotor preferentially accumulates near and moves along the edge of a physical/virtual boundary, the contour of which determines the motor trajectories. A few fundamental differences are, however, worth noting between steering by light patterns and by physical boundaries. First, physical boundaries confine a micromotor either because of steric hindrance or because of a complicated interplay among electrokinetics, chemical gradients, and hydrodynamics.[38,75,76] Such confinement only works for micromotors of specific types. Light patterns, on the other hand, confine micromotors via positive DEP and, in principle, work for a wider range of motors and even for inert particles that do not self-propel (see Figure S7). Second, a micromotor could reorient when approaching a boundary in both cases, but for different reasons: physical boundaries alter the orientation of an attracted motor by an interplay among different physical effects mentioned above, while light patterns generate a horizontal electric field that aligns a metallo-dielectric Janus particle. Last but not the least, a physical boundary is difficult to build and, even more so, to modify dynamically. Light patterns are, on the other hand, easy to be turned on and off and to reprogram, providing more flexibility for manipulating micromotors. For example, the various modes of motion of a micromotor—helical, spiral, and swarm transport—shown in Figure 5 would be quite challenging to achieve with a fixed, prefabricated microstructure.

Optoelectronic steering shown here can be applied to other micromotors as well. One intuitive requirement is that motors need to be more polarizable than the solution so that they undergo positive DEP and become trapped near the edges of the light pattern. Because metals are extremely polarizable in an electric field, any micromotor containing a reasonable amount of metal would satisfy this requirement. As an example, Figure 7 and Video S6 show that Au-Pt Janus microspheres, motors which move by catalytically decomposing H_2O_2 on their surfaces,[77,78] are confined at and move along the edge of a light pattern, in qualitatively the same way as a metallo-dielectric micromotor moving under AC electric fields. Interestingly, micromotors that experience negative DEP force (such as enzyme-coated dielectric particles[79−81]) could also be steered by the optoelectronic effect, by attracting them to dark patterns in an illuminated background. One interesting possibility is then to sort micromotors of different electrical polarizabilities via an optoelectronic setup, because those undergoing positive or negative DEP would move toward illuminated or dark regions, respectively.

Finally, the OET technology is an intriguing approach for investigating the behavior of micromotors in confinement.

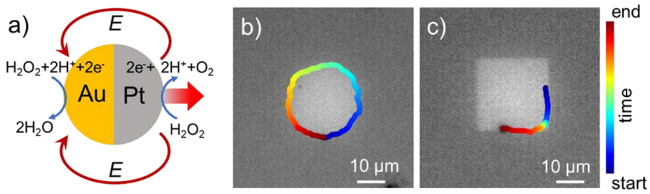

Figure 7. Steering a Au-Pt Janus micromotor in the OET system. (a) Schematic of a Au-Pt Janus microsphere moving by self-electrophoresis. (b and c) Trajectories of a Au-Pt micromotor confined by a circular (b) and square (c) light pattern. Experiments were performed in a 3 wt % H_2O_2 solution and under an AC electric field of 100 kHz.

Micromotors are primarily designed to function within confined microenvironments[82,83] such as blood vessels, porous tissue, and microfluidic chips, making it critical to explore how their propulsion changes with different sizes and geometries of confinement. The OET system, which creates a virtual confinement through a light pattern, offers a convenient and adaptable method to systematically investigate the effects of confined environments on micromotors. From a fundamental research standpoint, confinement can impact the self-organization process of micromotors.[84,85] By actively varying the OET confinement, both spatially and temporally, it becomes feasible to steer the self-organization of micromotors. This approach will improve our understanding of self-organization in biological systems and can be applied to develop techniques for controlling self-organization in artificial systems.

To further help our readers to assess the usefulness of the optoelectronic effect, we list the following requirements for the experimental setup. An electric field is required to produce the optoelectronic effect. AC electric fields are preferred over DC because AC fields are easy to handle, but not strictly necessary. A photoconductive substrate is also required, and hydrogenated amorphous Si is typically used. Light of appropriate wavelength is needed to activate the substrate. Finally, a device capable of generating dynamic light patterns is needed, such as the digital micromirror device (DMD) used in this work[86] or a specialized projector used in our recent work.[87,88] More details of the experimental setup can be found in the Methods, as well as in ref 42.

CONCLUSIONS

In summary, we have introduced a versatile and powerful strategy to steer micromotors using dynamic light patterns. This strategy is based on the optoelectronic effect, in which light illumination on a photoconductive substrate generates strong electric fields at the edge of light patterns. The resulting inhomogeneity of the electric field strength traps a micromotor via positive dielectrophoresis, so that it self-propels along the edge of the light pattern. An example is given for metallo-dielectric (SiO_2-Pt) micromotors moving via ICEP under AC electric fields oscillating at 100 kHz. Using static or dynamic light patterns, we were able to steer the trajectories and directionality of one or more micromotors, navigate them through complex environments, regulate their motion modes, and collect and transport them along programmable paths. Bimetallic, catalytically powered micromotors were also steered to showcase the generalizability of this technique.

Compared with other strategies for steering micromotors, such as those using magnetic fields,[89−92] physical boundaries,[32]

https://doi.org/10.1021/acsnano.2c12811
ACS Nano XXXX, XXX, XXX−XXX

or taxis,[30] optoelectronic steering is dynamic and reprogrammable and capable of manipulating single micromotors or their collectives. Moreover, because dielectrophoresis and the optoelectronic effect are universal, micromotors of a wide variety of propulsion mechanisms or physiochemical properties can be steered with high precision and tunability. Looking forward, we envision the optoelectronic steering of micromotors to greatly expand the usefulness of OET and provide opportunities for the precise and programmable control of a wide variety of micromotors in complex environments. However, optoelectronic steering also has its disadvantages, like requiring a specific photoconductive substrate. Thus, each steering approach possesses its own advantages and disadvantages, and it is more appropriate to compare and evaluate these methods of steering micromotors for a specific application scenario.

METHODS

Micromotor Fabrication. SiO_2 microspheres with a diameter of 5 μm were purchased from Tianjin Baseline Chrometch Research Center. Janus SiO_2-Pt microspheres were fabricated by sputtering a layer of Pt of 10 nm on a monolayer of SiO_2 microspheres. They were then sonicated off the substrate and dispersed in distilled water for later use. See Figure S1 for a scanning electron microscope image of a SiO_2-Pt Janus microsphere.

Experimental Setup. An optoelectronic tweezers device consists of two plates. The top plate is an ITO-coated glass slide from Riley Supplies. The bottom plate is an ITO-coated glass slide with an additional layer of 1 μm hydrogenated amorphous silicon (a-Si:H) deposited by plasma-enhanced chemical vapor deposition. An experimental chamber was made by placing on the bottom plate a silicone spacer of 200 μm thick with a circular hole of 5 mm in diameter. Then the suspension of micromotors was pipetted into the hole and the top plate was placed on the top of the silicone spacer to seal the chamber. The bottom plate and top plate were connected to a function generator (Agilent 33220A) with a power amplifier (Thurlby Thandor Instrument WA31). Unless otherwise noted, square waves of 100 kHz and a peak-to-peak voltage of 10 V were applied to drive the optoelectronic tweezers device. Light patterns were projected onto the a-Si:H layer of the device by a DMD-based light pattern projector (Mightex Polygon 1000G, 1100 mW LED source at 625 nm) through an upright optical microscope with a ×20 objective. (Nikon Eclipse Ni-E microscope integrated with a Märzhäuser Scan Plus 130−85 motorized stage).

Single-Particle Tracking. The motion of the micromotor was recorded by a CMOS camera (PCO Edge 4.2 CMOS monochromatic camera) typically at 25 frames per second (fps). These videos were then analyzed by homemade MATLAB codes to obtain the trajectories and instantaneous speeds of micromotors.

Fabrication of Physical Obstacles. Microstructures shown in Figure 5 in the main text were fabricated by standard photolithography. Photomask was designed using AutoCAD and then fabricated by exposing a chrome-on-glass substrate covered with AZ1500 photoresist using μPG 501 (Heidelberg) followed by development and etch steps. Briefly, photoresist (SU8 2005) was deposited on the bottom plate by spin coating at 1000 rpm for 30 s, followed by soft baking at 65 °C for 1 min and 105 °C for 4 min. The bottom plate with SU8 was then illuminated by a mask aligner (OAI model 30) with exposure energy of 180 mJ/cm^2 through the photomask to selectively photo-cross-link the SU8. Next, the bottom plate was baked at 65 °C for 1 min and 105 °C for 4 min and immersed in SU8 developer for 2 min with agitation to obtain the physical microstructures. After that, the bottom plate was rinsed with IPA and blow-dried with nitrogen, followed by hard baking at 150 °C for 5 min.

Numerical Simulations. A 3D finite element model was built in COMSOL Multiphysics (version 5.4) using the Electric Current module to simulate the distribution of electric potential and electric fields. Detailed information about this COMSOL model is given in the Supporting Information.

ASSOCIATED CONTENT

Supporting Information

The Supporting Information is available free of charge at https://pubs.acs.org/doi/10.1021/acsnano.2c12811.

SEM image of a SiO_2-Pt Janus microsphere, details on COMSOL simulation, results of the distributions of electrical potential and electric fields on the x-z cut plane, calculation of Clausius−Mossotti factor, explanation of using 0.1 mM NaCl liquid medium in our experiment, speeds of SiO_2-Pt micromotors undergoing ICEP under different driving voltages and at different electric field conditions, alignment of metallo-dielectric Janus microspheres in an electric field, both a SiO_2 microsphere and a SiO_2 microsphere coated with an Ag shell moving to the light pattern's edge under an AC electric field of 100 kHz, exhibiting positive dielectrophoresis, and two Janus SiO_2-Pt micromotors moving clockwise or counterclockwise in the circular light pattern under an AC electric field of 100 kHz (PDF)

Video S1: SiO_2-Pt micromotors undergoing ICEP in and outside light patterns, corresponding to Figure 1c, d in the main text (MP4)

Video S2: SiO_2-Pt micromotors accumulating at and moving along light patterns, corresponding to Figure 2b, c in the main text (MP4)

Video S3: SiO_2-Pt micromotors steered by static light patterns, corresponding to Figure 4 in the main text (MP4)

Video S4: Spiral, helical and linear motion of a micromotor in dynamic light patterns, corresponding to Figure 5 in the main text (MP4)

Video S5: Collection and transport of five SiO_2-Pt micromotors by a dynamic light pattern, corresponding to Figure 6 in the main text (MP4)

Video S6: Au-Pt micromotors confined by light patterns, corresponding to Figure 7 (MP4)

AUTHOR INFORMATION

Corresponding Authors

H. P. Zhang − *School of Physics and Astronomy and Institute of Natural Sciences, Shanghai Jiao Tong University, Shanghai 200240, China*; Email: hepeng_zhang@sjtu.edu.cn

Shuailong Zhang − *School of Mechatronical Engineering, Beijing Institute of Technology, Beijing 100081, China; Beijing Advanced Innovation Center for Intelligent Robots and Systems, Beijing Institute of Technology, Beijing 100081, China*; orcid.org/0000-0003-1004-021X; Email: shuailong.zhang@bit.edu.cn

Wei Wang − *Sauvage Laboratory for Smart Materials, School of Materials Science and Engineering, Harbin Institute of Technology (Shenzhen), Shenzhen 518055, China*; orcid.org/0000-0003-4163-3173; Email: weiwangsz@hit.edu.cn

Aaron R. Wheeler − *Institute of Biomedical Engineering, University of Toronto, Toronto M5S 3E1, Canada; Department of Chemistry, University of Toronto, Toronto M5S 3H6, Canada; Donnelly Centre for Cellular and Biomolecular Research, University of Toronto, Toronto M5S*

https://doi.org/10.1021/acsnano.2c12811
ACS Nano XXXX, XXX, XXX−XXX

3E1, Canada; orcid.org/0000-0001-5230-7475; Email: aaron.wheeler@utoronto.ca

Authors

Xi Chen − *Sauvage Laboratory for Smart Materials, School of Materials Science and Engineering, Harbin Institute of Technology (Shenzhen), Shenzhen 518055, China; Institute of Biomedical Engineering, University of Toronto, Toronto M5S 3E1, Canada; Department of Chemistry, University of Toronto, Toronto M5S 3H6, Canada; Donnelly Centre for Cellular and Biomolecular Research, University of Toronto, Toronto M5S 3E1, Canada*

Xiaowen Chen − *Sauvage Laboratory for Smart Materials, School of Materials Science and Engineering, Harbin Institute of Technology (Shenzhen), Shenzhen 518055, China*

Mohamed Elsayed − *Institute of Biomedical Engineering, University of Toronto, Toronto M5S 3E1, Canada; Donnelly Centre for Cellular and Biomolecular Research, University of Toronto, Toronto M5S 3E1, Canada*

Harrison Edwards − *Institute of Biomedical Engineering, University of Toronto, Toronto M5S 3E1, Canada; Department of Chemistry, University of Toronto, Toronto M5S 3H6, Canada*

Jiayu Liu − *Sauvage Laboratory for Smart Materials, School of Materials Science and Engineering, Harbin Institute of Technology (Shenzhen), Shenzhen 518055, China*

Yixin Peng − *Sauvage Laboratory for Smart Materials, School of Materials Science and Engineering, Harbin Institute of Technology (Shenzhen), Shenzhen 518055, China*

Complete contact information is available at: https://pubs.acs.org/10.1021/acsnano.2c12811

Author Contributions

X.C., S.Z., and W.W. conceived the idea. X.C., X.W.C., M.E., and H.E. carried out the experiments. X.C., J.L., and Y.P. fabricated and characterized the micromotors. X.C. and X.W.C. built the simulation model and ran the simulations. S.Z. and M.E. built the experimental setup and fabricated the OET devices. X.C. and W.W. wrote the manuscript. All authors discussed the results and commented on the manuscript. H.P.Z., S.Z., W.W., and A.R.W. coordinated and supervised the project.

Notes

The authors declare no competing financial interest.

ACKNOWLEDGMENTS

This work is supported by the Natural Science and Engineering Research Council of Canada (RGPIN 2019-04867, RTI-2019-00300), the Shenzhen Science and Technology Program (RCYX20210609103122038, JCYJ20190806144807401, JCYJ20210324121408022), and the National Natural Science Foundation of China (62103050, 12225410, 12074243). X.C. thanks the Chinese Government Scholarship (CSC No. 202106120280) for funding his study at University of Toronto. A.R.W. thanks the Canada Research Chairs program. We would like to acknowledge CMC Microsystems for the provision of products and services that facilitated this research, including the COMSOL license.

REFERENCES

(1) Wang, J. *Nanomachines: fundamentals and applications*; John Wiley & Sons: Weinheim, 2013.

(2) Chen, X.; Zhou, C.; Wang, W. Colloidal Motors 101: A Beginner's Guide to Colloidal Motor Research. *Chem. Asian J.* **2019**, *14* (14), 2388−2405.

(3) Mallouk, T. E.; Sen, A. Powering nanorobots. *Sci. Am.* **2009**, *300* (5), 72−77.

(4) Liu, T.; Xie, L.; Price, C.-A. H.; Liu, J.; He, Q.; Kong, B. Controlled propulsion of micro/nanomotors: operational mechanisms, motion manipulation and potential biomedical applications. *Chem. Soc. Rev.* **2022**, *51* (24), 10083−10119.

(5) Murai, R.; Ortiz, J.; Saeedi, S.; Kelly, P. H.; Davison, A. J. A robot web for distributed many-device localisation. *arXiv* **2022**, 2202.03314 (accessed Dec 7, 2022).

(6) Wang, W.; Lv, X.; Moran, J. L.; Duan, S.; Zhou, C. A practical guide to active colloids: choosing synthetic model systems for soft matter physics research. *Soft Matter* **2020**, *16* (16), 3846−3868.

(7) Aranson, I. S. Active colloids. *Phys.-Usp.* **2013**, *56* (1), 79.

(8) Das, M.; Schmidt, C. F.; Murrell, M. Introduction to active matter. *Soft Matter* **2020**, *16* (31), 7185−7190.

(9) Wang, W.; Zhou, C. A journey of nanomotors for targeted cancer therapy: principles, challenges, and a critical review of the state-of-the-art. *Adv. Healthcare Mater.* **2021**, *10* (2), 2001236.

(10) Li, H.; Peng, F.; Yan, X.; Mao, C.; Ma, X.; Wilson, D. A.; He, Q.; Tu, Y. Medical micro-and nanomotors in the body. *Acta Pharm. Sin. B* **2023**, *13* (2), 517−541.

(11) Xu, D.; Wang, Y.; Liang, C.; You, Y.; Sanchez, S.; Ma, X. Self-Propelled Micro/Nanomotors for On-Demand Biomedical Cargo Transportation. *Small* **2020**, *16* (27), 1902464.

(12) Kunti, G.; Wu, Y.; Yossifon, G. Rational Design of Self-Propelling Particles for Unified Cargo Loading and Transportation. *Small* **2021**, *17* (17), 2007819.

(13) Ying, Y.; Pumera, M. Micro/nanomotors for water purification. *Chem.—Eur. J.* **2019**, *25* (1), 106−121.

(14) Mallory, S. A.; Valeriani, C.; Cacciuto, A. An active approach to colloidal self-assembly. *Annu. Rev. Phys. Chem.* **2018**, *69*, 59−79.

(15) Teo, W. Z.; Pumera, M. Motion Control of Micro-/Nanomotors. *Chem.—Eur. J.* **2016**, *22* (42), 14796−14804.

(16) Tu, Y.; Peng, F.; Wilson, D. A. Motion manipulation of micro- and nanomotors. *Adv. Mater.* **2017**, *29* (39), 1701970.

(17) Jiang, J.; Yang, Z.; Ferreira, A.; Zhang, L. Control and Autonomy of Microrobots: Recent Progress and Perspective. *Adv. Intell. Syst.* **2022**, *4* (5), 2100279.

(18) Ebbens, S. J.; Gregory, D. A. Catalytic Janus colloids: controlling trajectories of chemical microswimmers. *Acc. Chem. Res.* **2018**, *51* (9), 1931−1939.

(19) Fusi, A. D.; Li, Y.; Llopis-Lorente, A.; Patiño, T.; van Hest, J. C.; Abdelmohsen, L. Achieving Control in Micro-/Nanomotor Mobility. *Angew. Chem., Int. Ed.* **2023**, *62* (5), e202214754.

(20) Al Harraq, A.; Bello, M.; Bharti, B. A guide to design the trajectory of active particles: From fundamentals to applications. *Curr. Opin. Colloid Interface Sci.* **2022**, *61*, 101612.

(21) Kline, T. R.; Paxton, W. F.; Mallouk, T. E.; Sen, A. Catalytic nanomotors: remote-controlled autonomous movement of striped metallic nanorods. *Angew. Chem., Int. Ed.* **2005**, *44* (5), 744−746.

(22) Ahmed, S.; Wang, W.; Mair, L. O.; Fraleigh, R. D.; Li, S.; Castro, L. A.; Hoyos, M.; Huang, T. J.; Mallouk, T. E. Steering acoustically propelled nanowire motors toward cells in a biologically compatible environment using magnetic fields. *Langmuir* **2013**, *29* (52), 16113−16118.

(23) Burdick, J.; Laocharoensuk, R.; Wheat, P. M.; Posner, J. D.; Wang, J. Synthetic nanomotors in microchannel networks: Directional microchip motion and controlled manipulation of cargo. *J. Am. Chem. Soc.* **2008**, *130* (26), 8164−8165.

(24) Dhar, P.; Cao, Y.; Kline, T.; Pal, P.; Swayne, C.; Fischer, T. M.; Miller, B.; Mallouk, T. E.; Sen, A.; Johansen, T. H. Autonomously moving local nanoprobes in heterogeneous magnetic fields. *J. Phys. Chem. C* **2007**, *111* (9), 3607−3613.

(25) Yang, F.; Mou, F.; Jiang, Y.; Luo, M.; Xu, L.; Ma, H.; Guan, J. Flexible Guidance of Microengines by Dynamic Topographical Pathways in Ferrofluids. *ACS Nano* **2018**, *12* (7), 6668−6676.

(26) Mou, F.; Xie, Q.; Liu, J.; Che, S.; Bahmane, L.; You, M.; Guan, J. ZnO-based micromotors fueled by CO2: the first example of self-reorientation-induced biomimetic chemotaxis. *Natl. Sci. Rev.* **2021**, *8* (11), nwab066.
(27) Lozano, C.; Ten Hagen, B.; Löwen, H.; Bechinger, C. Phototaxis of synthetic microswimmers in optical landscapes. *Nat. Commun.* **2016**, *7*, 12828.
(28) Chen, C.; Mou, F.; Xu, L.; Wang, S.; Guan, J.; Feng, Z.; Wang, Q.; Kong, L.; Li, W.; Wang, J.; Zhang, Q. Light-Steered Isotropic Semiconductor Micromotors. *Adv. Mater.* **2017**, *29*, 1603374.
(29) You, M.; Chen, C.; Xu, L.; Mou, F.; Guan, J. Intelligent micro/nanomotors with taxis. *Acc. Chem. Res.* **2018**, *51* (12), 3006−3014.
(30) Gao, C.; Feng, Y.; Wilson, D. A.; Tu, Y.; Peng, F. Micro-Nano Motors with Taxis Behavior: Principles, Designs, and Biomedical Applications. *Small* **2022**, *18* (15), 2106263.
(31) Liu, C.; Zhou, C.; Wang, W.; Zhang, H. Bimetallic microswimmers speed up in confining channels. *Phys. Rev. Lett.* **2016**, *117* (19), 198001.
(32) Katuri, J.; Caballero, D.; Voituriez, R.; Samitier, J.; Sanchez, S. Directed flow of micromotors through alignment interactions with micropatterned ratchets. *ACS Nano* **2018**, *12* (7), 7282−7291.
(33) Davies Wykes, M. S.; Zhong, X.; Tong, J.; Adachi, T.; Liu, Y.; Ristroph, L.; Ward, M. D.; Shelley, M. J.; Zhang, J. Guiding microscale swimmers using teardrop-shaped posts. *Soft Matter* **2017**, *13* (27), 4681−4688.
(34) Brown, A. T.; Vladescu, I. D.; Dawson, A.; Vissers, T.; Schwarz-Linek, J.; Lintuvuori, J. S.; Poon, W. C. Swimming in a crystal. *Soft Matter* **2016**, *12* (1), 131−140.
(35) Takagi, D.; Palacci, J.; Braunschweig, A. B.; Shelley, M. J.; Zhang, J. Hydrodynamic capture of microswimmers into sphere-bound orbits. *Soft Matter* **2014**, *10* (11), 1784−1789.
(36) Palacci, J.; Sacanna, S.; Vatchinsky, A.; Chaikin, P. M.; Pine, D. J. Photoactivated colloidal dockers for cargo transportation. *J. Am. Chem. Soc.* **2013**, *135* (43), 15978−15981.
(37) Yu, H.; Kopach, A.; Misko, V. R.; Vasylenko, A. A.; Makarov, D.; Marchesoni, F.; Nori, F.; Baraban, L.; Cuniberti, G. Confined Catalytic Janus Swimmers in a Crowded Channel: Geometry-Driven Rectification Transients and Directional Locking. *Small* **2016**, *12* (42), 5882−5890.
(38) Das, S.; Jalilvand, Z.; Popescu, M. N.; Uspal, W. E.; Dietrich, S.; Kretzschmar, I. Floor-or ceiling-sliding for chemically active, gyrotactic, sedimenting Janus particles. *Langmuir* **2020**, *36* (25), 7133−7147.
(39) Simmchen, J.; Katuri, J.; Uspal, W. E.; Popescu, M. N.; Tasinkevych, M.; Sánchez, S. Topographical pathways guide chemical microswimmers. *Nat. Commun.* **2016**, *7*, 10598.
(40) Das, S.; Garg, A.; Campbell, A. I.; Howse, J.; Sen, A.; Velegol, D.; Golestanian, R.; Ebbens, S. J. Boundaries can steer active Janus spheres. *Nat. Commun.* **2015**, *6*, 8999.
(41) Zhang, L.; Xiao, Z.; Chen, X.; Chen, J.; Wang, W. Confined 1D propulsion of metallodielectric Janus micromotors on microelectrodes under alternating current electric fields. *ACS Nano* **2019**, *13* (8), 8842−8853.
(42) Zhang, S.; Xu, B.; Elsayed, M.; Nan, F.; Liang, W.; Valley, J. K.; Liu, L.; Huang, Q.; Wu, M. C.; Wheeler, A. R. Optoelectronic tweezers: a versatile toolbox for nano-/micro-manipulation. *Chem. Soc. Rev.* **2022**, *51* (22), 9203−9242.
(43) Pankove, J.; Carlson, D. Electrical and optical properties of hydrogenated amorphous silicon. *Annu. Rev. Mater. Sci.* **1980**, *10* (1), 43−63.
(44) Wang, S.; Ma, F.; Zhao, H.; Wu, N. Bulk Synthesis of Metal−Organic Hybrid Dimers and Their Propulsion under Electric Fields. *ACS Appl. Mater. Interfaces* **2014**, *6* (6), 4560−4569.
(45) Zhang, J.; Alert, R.; Yan, J.; Wingreen, N. S.; Granick, S. Active phase separation by turning towards regions of higher density. *Nat. Phys.* **2021**, *17* (8), 961−967.
(46) Nishiguchi, D.; Sano, M. Mesoscopic turbulence and local order in Janus particles self-propelling under an ac electric field. *Phys. Rev. E* **2015**, *92* (5), 052309.
(47) Boymelgreen, A.; Yossifon, G. Observing electrokinetic Janus particle−channel wall interaction using microparticle image velocimetry. *Langmuir* **2015**, *31* (30), 8243−8250.
(48) Gangwal, S.; Cayre, O. J.; Bazant, M. Z.; Velev, O. D. Induced-charge electrophoresis of metallodielectric particles. *Phys. Rev. Lett.* **2008**, *100* (5), 058302.
(49) Bazant, M. Z.; Squires, T. M. Induced-charge electrokinetic phenomena. *Curr. Opin. Colloid Interface Sci.* **2010**, *15* (3), 203−213.
(50) Wu, J. ac electro-osmotic micropump by asymmetric electrode polarization. *J. Appl. Phys.* **2008**, *103* (2), 024907.
(51) Kolb, D. M. Electrochemical Surface Science. *Angew. Chem., Int. Ed.* **2001**, *40* (7), 1162−1181.
(52) Gangwal, S.; Cayre, O. J.; Bazant, M. Z.; Velev, O. D. Induced-Charge Electrophoresis of Metallodielectric Particles. *Phys. Rev. Lett.* **2008**, *100* (5), 058302.
(53) Ramos, A. *Electrokinetics and electrohydrodynamics in microsystems*; Springer Science & Business Media: Udine, 2011.
(54) Pethig, R. R. *Dielectrophoresis: Theory, methodology and biological applications*; John Wiley & Sons: West Sussex, 2017.
(55) Pethig, R. Dielectrophoresis: Status of the theory, technology, and applications. *Biomicrofluidics* **2010**, *4* (2), 022811.
(56) Gangwal, S.; Cayre, O. J.; Velev, O. D. Dielectrophoretic assembly of metallodielectric Janus particles in AC electric fields. *Langmuir* **2008**, *24* (23), 13312−13320.
(57) Velev, O. D.; Gangwal, S.; Petsev, D. N. Particle-localized AC and DC manipulation and electrokinetics. *Annu. Rep. Prog. Chem., Sect. C* **2009**, *105*, 213−246.
(58) Kilic, M. S.; Bazant, M. Z. Induced-charge electrophoresis near a wall. *Electrophoresis* **2011**, *32* (5), 614−628.
(59) Zhang, S.; Nikitina, A.; Chen, Y.; Zhang, Y.; Liu, L.; Flood, A. G.; Juvert, J.; Chamberlain, M. D.; Kherani, N. P.; Neale, S. L. Escape from an optoelectronic tweezer trap: experimental results and simulations. *Opt. Express* **2018**, *26* (5), 5300−5309.
(60) Chiou, P. Y.; Ohta, A. T.; Wu, M. C. Massively parallel manipulation of single cells and microparticles using optical images. *Nature* **2005**, *436* (7049), 370−372.
(61) Zhang, S.; Zhai, Y.; Peng, R.; Shayegannia, M.; Flood, A. G.; Qu, J.; Liu, X.; Kherani, N. P.; Wheeler, A. R. Assembly of Topographical Micropatterns with Optoelectronic Tweezers. *Adv. Opt. Mater.* **2019**, *7* (20), 1900669.
(62) Liang, W.; Liu, N.; Dong, Z.; Liu, L.; Mai, J. D.; Lee, G.-B.; Li, W. J. Simultaneous separation and concentration of micro-and nano-particles by optically induced electrokinetics. *Sens. Actuators A* **2013**, *193*, 103−111.
(63) Zhang, S.; Liu, Y.; Juvert, J.; Tian, P.; Navarro, J.-C.; Cooper, J. M.; Neale, S. L. Use of optoelectronic tweezers in manufacturing—accurate solder bead positioning. *Appl. Phys. Lett.* **2016**, *109* (22), 221110.
(64) Zhang, S.; Li, W.; Elsayed, M.; Tian, P.; Clark, A. W.; Wheeler, A. R.; Neale, S. L. Size-scaling effects for microparticles and cells manipulated by optoelectronic tweezers. *Opt. Lett.* **2019**, *44* (17), 4171−4174.
(65) Zhang, S.; Elsayed, M.; Peng, R.; Chen, Y.; Zhang, Y.; Peng, J.; Li, W.; Chamberlain, M. D.; Nikitina, A.; Yu, S. Reconfigurable multi-component micromachines driven by optoelectronic tweezers. *Nat. Commun.* **2021**, *12*, 5349.
(66) Zhang, S.; Scott, E. Y.; Singh, J.; Chen, Y.; Zhang, Y.; Elsayed, M.; Chamberlain, M. D.; Shakiba, N.; Adams, K.; Yu, S. The optoelectronic microrobot: A versatile toolbox for micromanipulation. *Proc. Natl. Acad. Sci. U. S. A.* **2019**, *116* (30), 14823−14828.
(67) Yang, W.; Yu, H.; Li, G.; Wang, Y.; Liu, L. High-throughput fabrication and modular assembly of 3D heterogeneous microscale tissues. *Small* **2017**, *13* (5), 1602769.
(68) Zhang, Y.; Zhao, J.; Yu, H.; Li, P.; Liang, W.; Liu, Z.; Lee, G.-B.; Liu, L.; Li, W. J.; Wang, Z. Detection and isolation of free cancer cells from ascites and peritoneal lavages using optically induced electrokinetics (OEK). *Sci. Adv.* **2020**, *6* (32), No. eaba9628.
(69) Ke, L.-Y.; Kuo, Z.-K.; Chen, Y.-S.; Yeh, T.-Y.; Dong, M.; Tseng, H.-W.; Liu, C.-H. Cancer immunotherapy μ-environment LabChip:

https://doi.org/10.1021/acsnano.2c12811
ACS Nano XXXX, XXX, XXX−XXX

taking advantage of optoelectronic tweezers. *Lab Chip* **2018**, *18* (1), 106−114.
(70) Chu, P.-Y.; Liao, C.-J.; Hsieh, C.-H.; Wang, H.-M.; Chou, W.-P.; Chen, P.-H.; Wu, M.-H. Utilization of optically induced dielectrophoresis in a microfluidic system for sorting and isolation of cells with varied degree of viability: Demonstration of the sorting and isolation of drug-treated cancer cells with various degrees of anti-cancer drug resistance gene expression. *Sens. Actuators B* **2019**, *283*, 621−631.
(71) Zhang, S.; Shakiba, N.; Chen, Y.; Zhang, Y.; Tian, P.; Singh, J.; Chamberlain, M. D.; Satkauskas, M.; Flood, A. G.; Kherani, N. P. Patterned optoelectronic tweezers: A new scheme for selecting, moving, and storing dielectric particles and cells. *Small* **2018**, *14* (45), 1803342.
(72) Wu, J.; Ben, Y.; Battigelli, D.; Chang, H.-C. Long-range AC electroosmotic trapping and detection of bioparticles. *Industrial & engineering chemistry research* **2005**, *44* (8), 2815−2822.
(73) Ramos, A.; Morgan, H.; Green, N. G.; Castellanos, A. AC electric-field-induced fluid flow in microelectrodes. *J. Colloid Interface Sci.* **1999**, *217* (2), 420−422.
(74) Chiou, P.-Y.; Ohta, A. T.; Jamshidi, A.; Hsu, H.-Y.; Wu, M. C. Light-actuated AC electroosmosis for nanoparticle manipulation. *J. Microelectromech. Syst.* **2008**, *17* (3), 525−531.
(75) Popescu, M. N.; Uspal, W. E.; Dominguez, A.; Dietrich, S. Effective interactions between chemically active colloids and interfaces. *Acc. Chem. Res.* **2018**, *51* (12), 2991−2997.
(76) Uspal, W.; Popescu, M. N.; Dietrich, S.; Tasinkevych, M. Self-propulsion of a catalytically active particle near a planar wall: from reflection to sliding and hovering. *Soft Matter* **2015**, *11* (3), 434−438.
(77) Wheat, P. M.; Marine, N. A.; Moran, J. L.; Posner, J. D. Rapid fabrication of bimetallic spherical motors. *Langmuir* **2010**, *26* (16), 13052−13055.
(78) Paxton, W. F.; Kistler, K. C.; Olmeda, C. C.; Sen, A.; St. Angelo, S. K.; Cao, Y.; Mallouk, T. E.; Lammert, P. E.; Crespi, V. H. Catalytic nanomotors: autonomous movement of striped nanorods. *J. Am. Chem. Soc.* **2004**, *126* (41), 13424−13431.
(79) Yuan, H.; Liu, X.; Wang, L.; Ma, X. Fundamentals and applications of enzyme powered micro/nano-motors. *Bioact. Mater.* **2021**, *6* (6), 1727−1749.
(80) Salinas, G.; Beladi-Mousavi, S. M.; Kuhn, A. Recent progress in enzyme-driven micro/nanoswimmers: From fundamentals to potential applications. *Curr. Opin. Electrochem.* **2022**, *32*, 100887.
(81) Mathesh, M.; Sun, J.; Wilson, D. A. Enzyme catalysis powered micro/nanomotors for biomedical applications. *J. Mater. Chem. B* **2020**, *8* (33), 7319−7334.
(82) Xiao, Z.; Wei, M.; Wang, W. A Review of Micromotors in Confinements: Pores, Channels, Grooves, Steps, Interfaces, Chains and Swimming in the Bulk. *ACS Appl. Mater. Interfaces* **2019**, *11* (7), 6667−6684.
(83) Wu, Z.; Chen, Y.; Mukasa, D.; Pak, O. S.; Gao, W. Medical Micro/Nanorobots in Complex Media. *Chem. Soc. Rev.* **2020**, *49* (22), 8088−8112.
(84) Bricard, A.; Caussin, J.-B.; Desreumaux, N.; Dauchot, O.; Bartolo, D. Emergence of macroscopic directed motion in populations of motile colloids. *Nature* **2013**, *503* (7474), 95−98.
(85) Araújo, N. A. M.; Janssen, L. M. C.; Barois, T.; Boffetta, G.; Cohen, I.; Corbetta, A.; Dauchot, O.; Dijkstra, M.; Durham, W. M.; Dussutour, A.; Garnier, S.; Gelderblom, H.; Golestanian, R.; Isa, L.; Koenderink, G. H.; Löwen, H.; Metzler, R.; Polin, M.; Royall, C. P.; Šarić, A.; Sengupta, A.; Sykes, C.; Trianni, V.; Tuval, I.; Vogel, N.; Yeomans, J. M.; Zuriguel, I.; Marin, A.; Volpe, G. Steering self-organisation through confinement. *Soft Matter* **2023**, *19* (9), 1695−1704.
(86) Zhang, S.; Li, W.; Elsayed, M.; Peng, J.; Chen, Y.; Zhang, Y.; Zhang, Y.; Shayegannia, M.; Dou, W.; Wang, T.; Sun, Y.; Kherani, N. P.; Neale, S. L.; Wheeler, A. R. Integrated Assembly and Photopreservation of Topographical Micropatterns. *Small* **2021**, *17* (37), 2103702.
(87) Chen, X.; Xu, Y.; Zhou, C.; Lou, K.; Peng, Y.; Zhang, H.; Wang, W. Unraveling the physiochemical nature of colloidal motion waves among silver colloids. *Sci. Adv.* **2022**, *8* (21), No. eabn9130.
(88) Chen, X.; Xu, Y.; Lou, K.; Peng, Y.; Zhou, C.; Zhang, H.; Wang, W. Programmable, Spatiotemporal Control of Colloidal Motion Waves via Structured Light. *ACS Nano* **2022**, *16* (8), 12755−12766.
(89) Garcia-Gradilla, V.; Orozco, J.; Sattayasamitsathit, S.; Soto, F.; Kuralay, F.; Pourazary, A.; Katzenberg, A.; Gao, W.; Shen, Y.; Wang, J. Functionalized Ultrasound-Propelled Magnetically Guided Nanomotors: Toward Practical Biomedical Applications. *ACS Nano* **2013**, *7* (10), 9232−9240.
(90) Hou, Y.; Wang, H.; Fu, R.; Wang, X.; Yu, J.; Zhang, S.; Huang, Q.; Sun, Y.; Fukuda, T. A review on microrobots driven by optical and magnetic fields. *Lab Chip* **2023**, *23* (5), 848−868.
(91) Zhou, H.; Dong, G.; Gao, G.; Du, R.; Tang, X.; Ma, Y.; Li, J. Hydrogel-Based Stimuli-Responsive Micromotors for Biomedicine. *Cyborg Bionic Syst.* **2022**, *2022*, 9852853.
(92) Li, J.; Dekanovsky, L.; Khezri, B.; Wu, B.; Zhou, H.; Sofer, Z. Biohybrid Micro- and Nanorobots for Intelligent Drug Delivery. *Cyborg Bionic Syst.* **2022**, *2022*, 9824057.

https://doi.org/10.1021/acsnano.2c12811
ACS Nano XXXX, XXX, XXX−XXX